Lawrence Berkeley National Laboratory

Lawrence Berkeley National Laboratory

Title

Pressure dependence of donor excitation spectra in AlSb

Permalink

https://escholarship.org/uc/item/1v7144x0

Authors

Hsu, L.
McCluskey, M.D.
Haller, E.E.

Publication Date

2002-01-16

eScholarship.org Powered by the California Digital Library
University of California

Pressure Dependence of Donor Excitation Spectra in AlSb

L. Hsu*
Department of Physics, University of California, Berkeley, California 94720
and Materials Sciences Division, Lawrence Berkeley National Laboratory, Berkeley, California 94720

M. D. McCluskey
Department of Physics and Institute for Shock Physics, Washington State University, Pullman, Washington 99164

E. E. Haller
Materials Sciences Division, Lawrence Berkeley National Laboratory, Berkeley, California 94720
and Department of Materials Science and Mineral Engineering, University of California, Berkeley, California 94720

PACS Numbers: 71.20.Nr, 71.55.Eq, 71.38.-k, 78.30.Fs

Abstract

We have investigated the behavior of ground to bound excited-state electronic transitions of Se and Te donors in AlSb as a function of hydrostatic pressure. Using broadband far-infrared Fourier transform spectroscopy, we observe qualitatively different behaviors of the electronic transition energies of the two donors. While the pressure derivative of the Te transition energy is small and constant, as might be expected for a shallow donor, the pressure derivatives of the Se transition energies are quadratic and large at low pressures, indicating that Se is actually a deep donor. In addition, at pressures between 30 and 50 kbar, we observe evidence of an anti-crossing between one of the selenium electronic transitions and a two-phonon mode.

*Present address: General College, University of Minnesota, Minneapolis, Minnesota 55455

I. Introduction

Aluminum antimonide (AlSb), an indirect gap III-V semiconductor with a bandgap of 1.7 eV, has been investigated as a candidate for several electronic and optoelectronic applications. For example, bulk AlSb has been considered as a possible material for infrared detectors[1] and optical holographic memories[2]. Epitaxial AlSb has been used as a component of resonant tunneling diodes[3] and infrared lasers[4], and also in combination with InAs to make Heterostructure Field Effect Transistors (HFETs) and High Electron Mobility Transistors (HEMTs)[5]. Despite these efforts, however, relatively little is known of the basic properties of AlSb. One reason for this is the extreme hygroscopicity of the material. Bulk samples of AlSb left exposed to open air disintegrate into powder in a matter of weeks, making special precautions necessary for its handling and storage. In this paper, we present results of an investigation to study the behavior of ground to bound excited-state transitions associated with Se and Te donors in AlSb under hydrostatic pressure.

It is well-known that hydrostatic pressure can be used to modify the band structure of semiconductors[6]. One way in which researchers have obtained information about semiconductor band structures under pressure is by studying the properties of impurity atoms. Previous studies have employed techniques such as photoluminescence, Hall effect, Raman spectroscopy, and magnetospectroscopy using lasers to study the effect of pressure on impurity states in a wide variety of semiconductors, including Si[7-10], GaP[11], Ge[12], GaAs[13-17], InP[18], InAs[19], CdTe[20], and ZnSe[21,22]. However, while such experiments can be used to determine the effect of hydrostatic pressure on the binding energy of impurity states, they cannot reveal any information about the behavior of the bound-excited states of those impurities. In a previous paper[23], we reported on a broadband-infrared spectroscopy study of ground to bound excited-state transitions of shallow

donors in GaAs at pressures under which GaAs became an indirect gap semiconductor with its conduction band minimum near the X symmetry point of the Brillouin zone. In contrast to the spectra of shallow donors in most semiconductors, in which several distinct electronic transition lines can be seen, only one transition line was observed for Si and Sn donors in indirect band gap GaAs, and only a broad continuum absorption was observed for S impurities[24]. We proposed that the reason for these unusual observations was that the X-point conduction band minimum in III-V semiconductors is not parabolic in shape, but instead has a "camel's back" structure[25]. We further demonstrated that such a band shape might admit only a limited number of bound excited-states, rather than the infinite number of such states allowed by a parabolic band. Because the conduction band minimum of AlSb is also located near the X symmetry point of the Brillouin zone and also has the camel's back shape[26], a study of donor spectra in this material might shed more light on the results obtained with GaAs under large hydrostatic pressure.

II. Experimental Techniques

The samples used in this experiment were small pieces of Se and Te doped AlSb, cut from single-crystal ingots grown by the Bridgman technique. The net doping concentration of the samples was 1-2 x 10^{16} cm^{-3}.

The pieces of AlSb were lapped to a thickness of about 50 μm and the surfaces were polished to a mirror-like finish using methanol and very fine grit. An ultrasonic grinder was used to cut out disk-shaped samples approximately 300 μm in diameter. These samples were then loaded into a modified Merrill-Basset diamond anvil cell (DAC)[27] along with a few grains of ruby powder which were included for purposes of measuring the pressure inside the cell. Liquid nitrogen, which has been shown to provide hydrostatic environments up to 130 kbar[28],

was used as a pressure medium. The pressure inside the cells at room temperature was determined by measuring the wavelength of one of the ruby fluorescence lines[29].

Measurements of the donor absorption spectra were performed at liquid helium temperatures using a Ge:Cu photoconductor. In order to focus as much light as possible through the small sample, the detector was mounted directly behind the cell and a light concentrating cone was attached to the front of the DAC[30]. The entire setup was placed inside a Janis STVP cryostat and infrared transmission measurements were performed using a Digilab FTS-80E Fourier-Transform spectrometer.

For the Se doped samples, a KBr beamsplitter and KBr cryostat windows were used. The pressure in the DAC at liquid helium temperatures was determined by the frequency of one of the vibrational modes of residual CO_2 molecules in the nitrogen pressure medium[31]. For the Te doped samples, a mylar beamsplitter and cryostat windows were used. In this case, the CO_2 vibrational mode was outside the observable spectral range and the pressure in the cell at low temperatures was estimated from the pressure at room temperature.

In AlSb, Se and Te donors have two stable configurations. One is the normal shallow donor state and the second is the deep DX state[32,33]. At atmospheric pressure, the DX center is the most stable form of Se and Te impurities. However, if these impurities are exposed to photons of sufficient energy, they can be transformed into the shallow donor configuration. At low temperatures (< ~100 K), a thermal barrier prevents their return to the DX state[34]. This bi-stability of the Se and Te donors in AlSb was exploited to obtain a good reference spectrum in order to produce an absorption spectrum that was free from instrumental and bulk material features.

Since DX centers are deep states which are spectroscopically inactive in the energy range studied, we used each sample as its own reference. The sample was first cooled under pressure in the dark so that the impurities would be in their DX configuration and a reference spectrum was taken. The infrared photons incident on the sample during this process did not possess enough energy to perturb the DX centers. Photons of much higher energy were then shined on the sample using an AlGaAs diode, converting the donors from their DX state into their shallow donor configuration, and a second spectrum was taken. An absorption spectrum was produced by taking the logarithm of the ratio of the spectra before and after exposure to photons from the AlGaAs diode.

III. Tellurium donors

Figure 1 shows the absorbance spectra of an AlSb:Te sample at three different hydrostatic pressures. Although many different absorbance lines have been seen in thicker samples[35], only the single line shown in figure 1 is large enough to be observed in the thin DAC samples. The broad absorption on the high energy side of the peak is due to electronic transitions from the Te ground state to higher bound-excited states (unresolved in this measurement) and also to the conduction band. This continuum absorption has also been seen in previous studies.

The one visible absorption line was previously ascribed to the 1s to $2p_{\pm}$ electronic transition of the Te donor because this transition always produces the strongest absorption line in the electronic spectra of shallow donors and the behavior of this absorption line under uniaxial stress is consistent with that of a 1s to $2p_{\pm}$ electronic transition[35]. The large width is most likely due to Stark broadening caused by the relatively large impurity concentration and is consistent

with linewidths found for electronic transitions associated with X-minimum donors in GaAs with a comparable doping level[23].

To determine the binding energy of the Te donor, we use the theory developed to calculate the ground and bound excited-state energy levels of donors associated with a camel's back minimum[25] and find that the energies of the four lowest electronic states relative to the conduction band minimum are –48.4 meV (1s), –22.2 meV ($2p_0$), –3.2 meV ($2p_\pm$), and –3.2 meV ($3p_0$). Because a donor-species-specific chemical shift affects the ionization energy of the 1s state much more than the 2p states, we estimate the binding energy of the Te donor by adding the 1s to $2p_\pm$ electronic transition energy to the theoretically calculated binding energy of the $2p_\pm$ state, obtaining a value of 66.7 meV at atmospheric pressure. Although the AlSb conduction band parameters used to calculate this energy are extrapolated from GaP[26], rather than measured, this value is close to the binding energy of 68 meV previously obtained through Hall effect measurements[36].

When hydrostatic pressure is applied, the energy of this electronic transition decreases. Figure 2 shows the peak position as a function of the room-temperature cell pressure. As mentioned above, because of the spectral range in which this transition falls, we could not directly measure the pressure in the cell at the low temperatures at which the spectra were taken. The pressures plotted are the room temperature cell pressures obtained by a ruby fluorescence measurement. Because the cell pressure changes upon cooling due to differential thermal contraction of the different parts of the cell, the room-temperature pressures are only an estimate of the actual cell pressures during the measurements. From prior experience working with these particular DACs, the actual pressure in the cell at liquid helium temperatures could differ from the room temperature pressure by as much as 10 kbar. Thus, the scatter in the data is most likely

due to uncertainties in the actual cell pressure at low temperatures. Despite the scatter, it is evident that the peak energy decreases with increasing pressure.

Two measurements were made at very low pressures (0 and 4.1 kbar) using a combination of cryostat windows and beamsplitter which did allow an *in situ* pressure measurement. These points are indicated by squares, rather than circles, in the graph. Because the transition energies are nearly identical at both these pressures, the shift of the transition energy may be different at low pressures than at high pressures.

A linear fit to the high pressure data yields

$$\omega = 62.5 meV - 0.13 \frac{meV}{kbar} P \qquad (1)$$

where ω is the transition energy and P is the applied hydrostatic pressure. Because of the unaccounted pressure offset, this fit does not intersect the known energy of the transition line at atmospheric pressure.

It is possible to calculate the pressure dependence of the Te binding energy based on the energy of this transition and a knowledge of the pressure dependencies of the effective mass, dielectric constant, and other parameters. However, such a calculation would be quite unreliable because of the lack of such data for AlSb. Since the continuum absorption on the high-energy side of the peak shifts with the peak itself, one can infer that the pressure dependence of the Te donor binding energy is roughly the same as the pressure dependence of the 1s to $2p_{\pm}$ electronic transition (–0.13 meV/kbar). In table 1, we compare the pressure dependence of the binding energies of shallow impurities in several different semiconductors. The pressure dependence of the Te donor in AlSb is somewhat larger than, but still comparable to the pressure dependence of the binding energies of shallow impurities in other materials, such as Si. Such small linear shifts of the impurity binding energies in other semiconductors are attributed to changes in the

effective mass and dielectric constant of those materials as a function of pressure[7]. Although the pressure dependencies of the effective mass and dielectric constant in AlSb are unknown, it seems reasonable that such a small pressure derivative of the Te binding energy could be similarly accounted for by the changes in those quantities.

IV. Selenium donors

A. Pressure dependence

The electronic transition spectrum of Se donors in AlSb at atmospheric pressure is shown in figure 3. Two strong absorption lines at 117 meV and 139 meV are seen, one of which lies on the shoulder of a continuum absorption band. Both lines and the continuum have previously been observed in bulk samples and have been identified as caused by the Se donor[35]. As is the case in the Te-doped samples, the continuum absorption arises from transitions from the Se ground state to the conduction band and as was seen in the spectra of bulk samples, the strength of the continuum absorption relative to the discrete electronic transitions is much larger for the Se donor than for the Te donor.

We assign the lower energy peak to the 1s to $2p_0$ electronic transition and the higher energy peak to the 1s to $2p_\pm$ for the following reasons: (1) these two transitions always produce the most intense lines in the absorption spectra of shallow donors, (2) the observed energy separation of the two transition lines is 21.5 meV, closest to the calculated separation of 19 meV between the $2p_0$ and $2p_\pm$ states (with binding energies of –22.2 meV and –3.2 meV, respectively), and (3) observations of the behavior of these transition lines under uniaxial stress in other experiments are consistent with the given assignments[35]. Although theoretically, the $2p_\pm$ and $3p_0$

states are degenerate, the splitting of the higher energy transition line is consistent with a 1s to $2p_{\pm}$, and not a 1s to $3p_0$ transition.

Previously, the lower energy peak was assigned to a $1s(A_1)$ to $1s(T_1)$ transition because its behavior under uniaxial stress is also consistent with such a transition and because assigning the two lines observed here to 1s to $2p_0$ and 1s to $2p_{\pm}$ transitions would have led to excited-state energy separations which were too far out of line with the theoretical results predicted by Faulkner's effective mass theory model[35]. However, recognition that the intensity of this line is too large relative to the 1s to $2p_{\pm}$ transition line (compared to such observed transitions in other semiconductor systems) and the use of the correct camel's back model to calculate the energies of the bound-excited states of the impurity allow us to assign these lines properly.

Following the same procedure as used to determine the ground state energy of the Te donor, we find the binding energy of the Se donor electron to be about 140 meV. This is somewhat different from the value of 160 meV obtained from Hall effect measurements[36]. However, again it must be remembered that the conduction band parameters used in the theoretical calculation are not very well known.

Figure 3 also shows a series of Se donor spectra at low pressures. As was the case with the Te donor, the electronic transition peaks shift to lower energies as the pressure is increased. However, something strange happens to the 1s to $2p_{\pm}$ transition line. As the pressure increases from atmospheric pressure to 7 kbar, the 1s to $2p_{\pm}$ transition becomes less and less distinct from the continuum. At 7 kbar, only a small shoulder on the rising edge of the continuum absorption remains. As the pressure is increased further, this peak once again reappears. This phenomenon was reproducible and at present, the reason for this behavior is unknown. Because the 1s to $2p_0$ transition remains clearly distinct throughout this pressure regain,, it seems unlikely that this

disappearance could be due to non-uniform pressure on the sample. In addition, visual observation showed that the sample was not in contact with the diamonds, gasket, or ruby grains at more than one point.

Plotting the energies of the two transitions lines as a function of applied pressure yields the plot shown in figure 4. Because of the spectral range in which these lines are found, the vibrational mode of residual CO_2 dissolved in the nitrogen pressure medium could be observed and was used to determine the pressure in the cell at the low temperatures at which the measurements were made[31]. Thus, the uncertainty in the pressure and the scatter in the data is much less than in the AlSb:Te study. Again, the continuum absorption shifts with the transition lines, indicating that the binding energy of the Se donor shifts at the same or nearly the same rate as the energies of the ground to bound excited-state transitions. A third peak, whose energies are labeled "III" in figure 4, begins to appear at about 30 kbar, and it will be discussed later.

Comparing figures 2 and 4, two large differences in the behaviors of the Te and Se donors under hydrostatic pressure become apparent. Not only are the pressure derivatives of the transition energies qualitatively different (linear vs. non-linear), but at atmospheric pressure, the magnitude of the pressure derivative of the energy of the Se transitions is more than 10 times larger than that of the Te transition and is comparable to the pressure derivative of the bandgap energy ($dE_{gap}/dP = -4.2$ meV/kbar[37]). As one can see in table 1, such a large pressure dependence is more similar to the pressure dependencies of deep levels, such as gold in germanium or gold and the group VI elements in silicon. According to modern definitions of "shallow" and "deep" levels, where impurities are classified by the pressure derivatives of their binding energies rather than their binding energies themselves[9,10,38], selenium should thus be classified as a deep donor in AlSb. The selenium donor electron is localized near the impurity

site and is bound by the short-range impurity potential, rather than a long-range screened Coulomb potential. Thus, the pressure derivative of its binding energy will depend on the behavior of the entire conduction band, in addition to higher bands. In one previous calculation, selenium was predicted to form a deep level in AlSb with a binding energy pressure derivative of –1 meV/kbar[39].

While the pressure dependence of the ionization energies of the majority of impurities have been reported to be linear, many of these dependencies have been measured only at low pressures (up to 10 kbar or less)[7,9,10,12,19]. Higher pressure measurements of Si:Au[8], CdTe:Sb[20], and n-type InP under high magnetic fields[17] indicate that some impurity levels also vary non-linearly with pressure. While one may speculate that such non-linear dependencies are due to the influence of short range impurity potentials, the theory is not yet well-developed enough to explain this effect. At the highest pressures measured in the current experiments, in which the Se binding energy becomes comparable to the binding energy of the Te donor at atmospheric pressure, the pressure derivative of the Se binding energy decreases to roughly –0.2 meV/kbar, comparable to the pressure derivative of the Te binding energy. It is possible that the application of hydrostatic pressure causes the delocalization of the Se donor electron wavefunction to the extent where Se becomes a shallow impurity.

B. Anti-crossing behavior

As was mentioned above, at around 30 kbar, a third peak, labeled “III” in figure 4, begins to appear in the spectrum. Figure 5 shows Se donor spectra near and above this pressure, showing the emergence of this third peak. The slanted arrows show the 1s to $2p_0$ and 1s to $2p_\pm$ electronic transition peaks while the vertical arrow points to the emerging third peak. At these

higher pressures, the electronic transition peaks are significantly broadened, though the reason for this is not known. In particular, the feature we assign to the 1s to $2p_{\pm}$ electronic transition is not readily identifiable as an electronic transition peak. However, we believe that it is, in fact, the 1s to $2p_{\pm}$ transition because (1) its width is always about the same as that of the 1s to $2p_0$ electronic transition, (2) the energy of this feature and its pressure dependence connect smoothly to that of the 1s to $2p_{\pm}$ electronic transition at lower pressures (see figure 4), and (3) visual observation of a series of spectra at different pressures indicates that this is indeed the 1s to $2p_0$ electronic transition peak.

It is clear from the spectra in figure 5 that (1) this third peak increases in intensity as the pressure is increased and (2) at a pressure of 50 kbar (and above, in spectra which are not shown), this third peak resembles the 1s to $2p_{\pm}$ transition which was seen at low pressures. This behavior suggests that the origin of the third peak might be an additional level which interacts with the 1s to $2p_{\pm}$ electronic transition. Figure 6 shows how another level, whose frequency increases slightly with pressure, might interact with the 1s to $2p_{\pm}$ electronic transition to produce an anti-crossing which closely approximates the observations. Searching through the literature to find possible sources of such levels, we find that a two-optical-phonon mode is a possible candidate. Although the two-phonon energies and pressure dependencies have not been measured, the energies and pressure derivatives of the AlSb optical phonons are well-known[40].

An anti-crossing occurs when the unperturbed energies of two levels cross each other as a result of applying some perturbation, such as hydrostatic pressure, uniaxial stress, or a magnetic field. In AlSb:Se, as hydrostatic pressure is applied, the energy of the two optical phonon modes increase and the energy of the 1s to $2p_{\pm}$ electronic transitions decrease, the two levels crossing at about 40 kbar. If the two levels interact repulsively, then the energies of each will be perturbed

so as to avoid crossing each other. Such a phenomenon is not rare in semiconductor physics and has been observed between two vibrational modes[41,42], two electronic transitions[43,44], and between an electronic transition and a vibrational mode[45-49]. Whether or not the two levels interact is determined by their symmetries and the requirement of the conservation of energy. In this case, an interaction between an electronic transition and a two-phonon mode can be thought of as a process in which the decay of a bound impurity electron from the $2p_{\pm}$ state to the 1s state results in the emission of two optical phonons with a combined energy equal to the energy difference between the two donor levels (the one-phonon modes are too low in energy to be able to interact with this electronic transition). Because the symmetry of the $2p_{\pm}$ bound-excited state is $2T_1 + 2T_2$, the vibrational mode with which the electronic transition interacts must have either T_1 or T_2 symmetry.

To calculate the effects of such an interaction quantitatively, we must calculate the energies of the two-optical phonon modes in AlSb. Although no data regarding the pressure dependence of two-phonon modes in AlSb exists, the energies of the zone center one-phonon LO and TO modes have been measured as a function of hydrostatic pressure[40]. By forming additive combinations of these frequencies, the energies of the two-phonon optical modes can be estimated.

We use a simple two-level model to calculate the effects of an interaction between the 1s to $2p_{\pm}$ electronic transition and a two-phonon mode. The total Hamiltonian of this system is given by

$$H = H_{elec} + H_{pho} + H_{\text{int}}, \qquad (2)$$

where H_{elec} and H_{pho} are the Hamiltonians for the electronic transition and the two-phonon mode respectively and H_{int} describes the interaction between these two systems. If we treat H_{int} as a weak perturbation, then the Hamiltonian matrix can be written as

$$H = \begin{bmatrix} \omega_{elec} & A \\ A & \omega_{phon} \end{bmatrix} \tag{3}$$

where ω_{elec} and ω_{phon} are the energies of the unperturbed electronic transition and two-phonon mode and

$$A = \left\langle n_{pho}, \psi_{2p_{\pm}} \middle| H_{\text{int}} \middle| n+1_{pho}, \psi_{1s} \right\rangle. \tag{4}$$

Using simple degenerate perturbation theory to diagonalize this Hamiltonian, we obtain

$$\omega_{\pm} = \frac{1}{2}\left(\omega_{elec} + \omega_{pho} \pm \sqrt{\left(\omega_{elec} - \omega_{pho}\right)^2 + 4A^2}\right) \tag{5}$$

for the new eigenenergies of this system. The wavefunctions corresponding to eigenstates of this Hamiltonian are no longer pure electronic transitions or pure two-phonon excitations, but a mixture of the two given by

$$|\psi\rangle = a\,|\psi_{elec}\rangle + b\,|\psi_{pho}\rangle, \tag{6}$$

where the square modulus of the coefficient a is

$$|a|^2 = \frac{A^2}{\left(\omega_{pho} - \omega\right)^2 + A^2} \tag{7}$$

The quantity $|a|^2$ is the normalized area of the absorption peak.

To calculate the energies of the perturbed levels, we must first find the energies of the unperturbed electronic transition and optical phonon modes. The energy of the unperturbed 1s to $2p_{\pm}$ electronic transition is estimated by fitting the energies of the 1s to $2p_{\pm}$ electronic transition at low energies and the energies of the third peak (III) at pressure of 50 kbar and above, where it

resembles the 1s to $2p_{\pm}$ electronic transition peak. This is the upper dashed curve in figure 6 and is given by

$$\omega\,(1s \rightarrow 2p_{\pm}) \;=\; 137.4\,meV \;-\; 1.77\frac{meV}{kbar}P \;+\; 0.013\frac{meV}{kbar^2}P^2. \qquad (8)$$

The energy of the interacting two-phonon mode is taken to be

$$\omega_{pho} \;=\; 81.5\,meV \;+\; 0.138\frac{meV}{kbar}P \;-\; 0.00024\frac{meV}{kbar^2}P^2 \qquad (9)$$

which is obtained by adding the energies of the one-phonon LO and TO modes[40]. We choose this combination because, of the three possible two-phonon combinations (2 LO, 2 TO, and LO + TO), the LO + TO combination produces the best fit to the data. Due to anharmonic terms, equation (9) likely overestimates the frequency of the LO + TO mode and may be closer to the true frequency of the 2 LO mode. Of course, two-phonon modes have a range of energies and any mode which has an energy close to the electronic transition energy, a total k-vector of nearly zero (electronic transitions involve a negligible change in momentum), and the proper symmetry can participate in the interaction.

The new eigenenergies of the two levels obtained from equations (5), (8) and (9) are plotted in figure 6 along with the experimentally observed energies. The interaction parameter of A = 25 cm^{-1} is obtained by adjusting it to produce the best fit between theory and experiment. As the pressure is increased, the lower branch, which is initially "phonon-like," acquires more of the characteristics of an electronic transition, becoming "electronic-transition like." Similarly, the upper branch which is initially "electronic-transition-like," becomes more "phonon-like" at high pressures. In the process, spectral intensity is transferred from one level to the other.

Our two-level model can also be used to predict intensities of the absorption lines of the two levels. Figure 7 shows the measured area of the lower-energy peak along with the

theoretical prediction from equation (7). Naturally, the same value of 25 cm^{-1} was used for *A* in the calculation of the theoretical curve. Since the original 1s to $2p_{\pm}$ electronic transition peak is difficult to track because it is located on the leading edge of a continuum absorption, the area of this lower branch peak was normalized to that of the 1s to $2p_0$ transition. Thus, we implicitly assume that the relative areas of the two electronic transition peaks remain constant as the pressure is increased. The fit is not quite as good as the one for the transition energies, but has qualitatively the correct shape.

It should be noted that only a single free parameter (*A*) is used in this model to fit both the energies of the interacting levels and the intensities of the resulting absorptions. Although the interaction of the phonons with the 1s to $2p_{\pm}$ transition is quite large, it is not known why no interaction of these phonons with the 1s to $2p_0$ transition is observed. One possibility is that the two-phonon mode has T_2 symmetry, which would allow it to interact with the 1s to $2p_{\pm}$ transition ($2T_1 + 2T_2$ symmetry), but not the 1s to $2p_0$ transition ($A_1 + E + T_1$ symmetry). It is also possible that the interaction parameter of the phonon mode with the 1s to $2p_0$ transition is too small for an interaction to be observed in our experiment.

V. Conclusions

We have used Fourier transform infrared spectroscopy to study the behavior of Se and Te donors in AlSb under hydrostatic pressure. Only one or two electronic transitions were observed, similar to the absorption spectra for shallow donors associated with the X conduction band minimum in GaAs, where only one electronic transition was seen.

We find the ionization energy of the Te donor to be 66.7 meV and that this energy changes linearly at the rate of roughly –0.13 meV/kbar with applied hydrostatic pressure. This behavior is similar to that of hydrogenic impurities in other semiconductors.

In contrast, the ionization energy of the Se donor is roughly 140 meV and decreases quadratically with applied hydrostatic pressure. The pressure derivative of the binding energy ranges from –1.8 meV/kbar at low pressures to –0.2 meV/kbar at high pressures. Such a large slope at low pressures is comparable to the shifts of deep centers in other semiconductors and suggests that at atmospheric pressure, selenium is also a deep center in AlSb with a binding energy which is determined by the short range impurity potential of the selenium atom. As the applied hydrostatic pressure is increased, the selenium center appears to undergo a smooth deep-shallow transition, until at high pressures, its binding energy has only a small pressure derivative.

The spacing between the two electronic transition lines associated with the Se donor and their assignments based on previous uniaxial stress studies support the suggestion that the conduction band minimum near the X symmetry point has a “camel’s back shape” rather than a parabolic shape like the conduction band minimum in silicon since this spacing is predicted rather well by the camel’s back theory and poorly by the usual effective mass theory.

Finally, we propose a model in which the 1s to $2p_{\pm}$ electronic transition of the Se impurity interacts with a two-phonon mode to explain the growth and pressure dependence of an anomalous third line in the absorption spectra. A simple two-level perturbation calculation with a single parameter allows us to explain both the energies of the interacting levels and the changes in intensity of the absorption lines.

Acknowledgements

We are indebted to A. K. Ramdas at Purdue University for supplying the doped AlSb samples used in this study. The diamond-anvil cell and photoconductors used in this investigation were designed and constructed by J. Wolk and J. Beeman. This work was supported in part by NSF Grant No. DMR-0109844, by Director, Office of Science, Office of Basic Energy Sciences, Division of Materials Sciences and Engineering, of the U.S. Department of Energy under Contract No. DE-AC03-76SF00098, and by the Office of Naval Research. The work at WSU was supported by NSF Grant No. DMR-9901625.

References

1. B. Brar, L. Samoska, H. Kroemer, and J. H. English, J. Vac. Sci. and Tech. B **12**, 1242 (1994).
2. J. M. McKenna, D. D. Nolte, W. Walukiewicz, and P. Becla, Appl. Phys. Lett. **68**, 735 (1996).
3. D. H. Chow, H. L. Dunlap, W. Williamson, S. Enquist, B. K. Gilbert, S. Subramaniam, P. M. Lei, and G. H. Bernstein, IEEE Electron Device Lett. **17**, 69 (1996).
4. J. R. Meyer et al., IEE Proc.-J: Optoelectron. **145**, 275 (1998).
5. C. R. Bolognesi and D. H. Chow, IEEE Elec. Dev. Lett. **17**, 534 (1996).
6. C. J. Armistead, F. Kuchar, S. P. Nadja, S. Porowski, C. Sotomayor-Torres, R. A. Stradling, Z. Wasilewski, *Proceedings of the 17th International Conference on the Physics of Semiconductors, San Francisco, 1984* (Springer-Verlag, New York, 1985), pp. 1047-50.
7. M. G. Holland and W. Paul, Phys. Rev. **128**, 30 (1962).
8. M.I. Nathan and W. Paul, Phys. Rev. **128**, 38 (1962).
9. G. A. Samara and C. E. Barnes, Phys. Rev. **B 35**, 7575 (1987).
10. W. Jantsch, K. Wünstel, O. Kumagai, and P. Vogl, Phys. Rev. **B 25**, 5515 (1982).
11. P. Galtier and G. Martinez, Solid State Commun. **65**, 193 (1988).
12. M. G. Holland and W. Paul, Phys. Rev. **128**, 43 (1962).
13. D. J. Wolford and J. A. Bradley, Solid State Commun. **53**, 1069 (1985).
14. J. E. Dmochowski, R. A. Stradling, P. D. Wang, S. N. Holmes, M. Li, B. D. McCombe, and B. Weinstein, Semicond. Sci. Technol. **6**, 476 (1991).
15. J. Leymarie, M. Leroux, and G. Neu, Phys. Rev. **B 42**, 1482 (1990).

16. X. Liu, L. Samuelson, M.-E. Pistol, M. Gerling, and S. Nilsson, Phys. Rev. **B 42**, 11791 (1990).

17. N. Lifshitz, A. Jayaraman, R. A. Logan, and H. C. Card, Phys. Rev. **B 21**, 670 (1980)

18. A. Kadri, K. Zitouni, L. Konczewicz, and R. L. Aulombard, Phys. Rev. **B 35**, 6260 (1987).

19. A. Kadri, R. L. Aulombard, K. Zitouni, M. Baj, and L. Konczewicz, Phys. Rev. **B 31**, 8013 (1985).

20. M. Prakash, M. Chandrawsekhar, H. R. Chandrasekhar, I. Miotkowski, and A. K. Ramdas, Phys. Rev. **B 42**, 3586 (1990).

21. T. M. Ritter, B. A. Weinstein, R. M. Park, and M. C. Tamargo, Phys. Rev. Lett. **76**, 964 (1996).

22. I. L. Kuskovsky, G. F. Neumark, J. G. Tischler, and B. A. Weinstein, Phys. Rev. **B 63**, 161201(R) (2001).

23. L. Hsu, S. Zehender, E. Bauser, and E. E. Haller, Phys. Rev. **B 55**, 10515 (1997).

24. L. Hsu, Ph.D thesis, University of California, Berkeley, unpublished.

25. A. A. Kopylov and A. N. Pikhtin, Sov. Phys. Semicond. **11**, 510 (1977).

26. A. A. Kopylov, Solid State Comm. **56**, 1 (1985).

27. J. A. Wolk, M. B. Kruger, J. N. Heyman, W. Walukiewicz, R. Jeanloz, E. E. Haller, Phys. Rev. Lett. **66**, 774 (1991).

28. R. LeSar, S. A. Ekberg, L. H. Jones, R. L. Mills, L. A. Schwalbe, D. Schiferl, Solid State Communications **32**, 131 (1979).

29. G. J. Piermiani, S. Block, J. D. Barnett, and R. A. Forman, J. Appl. Phys. **46**, 2774 (1975).

30. J. A. Wolk, M. B. Kruger, J. N. Heyman, J. W. Beeman, J. G. Guitron, E. D. Bourret, W. Walukiewicz, R. Jeanloz, E. E. Haller, Materials Science Forum **83-87,** 757 (1992).

31. M. D. McCluskey, L. Hsu, L. Wang, and E. E. Haller, Phys. Rev. B **54**, 8962 (1996).

32. W. Jost, M. Kunzer, U. Kaufmann, and H. Bender, Phys. Rev. B **50**, 4341 (1994).

33. P. Becla, A. Witt, J. Lagowski, and W. Walukiewicz, Appl. Phys. Lett. **67**, 395 (1995).

34. D. V. Lang and R. A. Logan, Phys. Rev. Lett. **39**, 635 (1977).

35. B. T. Ahlburn and A. K. Ramdas, Phys. Rev. **167**, 717 (1968).

36. W. J. Turner and W. E. Reese, Phys. Rev. **117**, 1003 (1960).

37. K. Strössner, S. Ves, C. K. Kim, and M. Cardona, Phys. Rev. **B 33**, 4044 (1986).

38. H. P. Hjalmarson, P. Vogl, D. J. Wolford, and J. D. Dow, Phys. Rev. Lett. **44**, 810 (1980).

39. R. D. Hong, D. W. Jenkins, S. Y. Ren, and J. D. Dow, Phys. Rev. **B 38**, 12549 (1988).

40. S. Ves, K. Strössner and M. Cardona, Solid State Comm. **57**, 483 (1986).

41. A. Göbel, T. Ruf, A. Fischer, K. Eberl, M. Cardona, J. P. Silveira and F. Briones, Phys. Rev. **B 59**, 12612 (1999).

42. A. Fainstein, M. Trigo, D. Oliva, B. Jusserand, T. Freixanet and V. Thierry-Mieg, Phys. Rev. Lett. **86**, 3411 (2001).

43. L. Brunel, S. Huant, M. Baj, and W. Trzeciakowski, Phys. Rev. **B 33**, 6863 (1986).

44. S. Bednarek and J. Adamowski, Phys. Rev. **B 51**, 4687 (1995).

45. J. T. Devreese, J. De Sitter, E. J. Johnson, and K. L. Ngai, Phys. Rev. **B 17**, 3207 (1978).

46. E. J. Johnson and D. M. Larsen, Phys. Rev. Lett. **16**, 655 (1966).

47. R. Kaplan, K. L. Ngai, and B. W. Henvis, Phys. Rev. Lett. **28**, 1044 (1972).

48. D. R. Cohn, D. M. Larsen, and B. Lax, Phys. Rev. **B 6**, 1367 (1972).

49. M. Nakayama, J. Phys. Soc. Jpn. **27**, 636 (1969).

Figure and Table Captions

Table 1 Pressure dependence of impurity binding energies in various materials.

Fig. 1 Absorption spectra of AlSb:Te at three different hydrostatic pressures. The largest single peak is assigned to the 1s to $2p_{\pm}$ electronic transition.

Fig. 2 Energy of the 1s to $2p_{\pm}$ transition line in AlSb:Te as a function of pressure. Pressures for the two square points were measured *in situ* at low temperature while pressures for the points indicated by circles were measured at room temperature. The line is a linear fit to the high pressure points.

Fig. 3 AlSb:Se donor spectra at low pressures showing the disappearance and re-emergence of the 1s to $2p_{\pm}$ electronic transition peak. The higher energy peak nearly disappears into the continuum around 7 kbar, then reappears as the pressure is increased further. The vertical arrow tracks the 1s to $2p_{\pm}$ electronic transition.

Fig. 4 Pressure dependence of the electronic transition peaks in AlSb:Se. A third peak (indicated by the triangles and labeled III) begins to appears at about 30 kbar. The lines are included as guides to the eye.

Fig. 5 Spectra of AlSb:Se showing the emergence and growth of the third peak as the pressure is increased. The slanted arrows indicate the 1s to $2p_0$ and 1s to $2p_{\pm}$ electronic transitions, and the

vertical arrows point to the emerging third peak. At 50 kbar, the emerging peak resembles the original 1s to $2p_{\pm}$ electronic transition peak (compare with the spectra in figure 4).

Fig. 6 Comparison of the energies predicted by the two-level anti-crossing model discussed in the text with observed data. The dashed curves are the unperturbed energies of the 1s to $2p_{\pm}$ electronic transition and a two-phonon mode. The solid curves are the perturbed energies calculated from equation (5). The circles and triangles are the experimentally measured frequencies of the relevant absorption lines.

Fig. 7 Pressure dependence of the area of peak III. The circles are the measured peak areas normalized to the area of the 1s to $2p_0$ electronic transition peak. The curve is calculated from equation (7), assuming that the oscillator strengths of both electronic transitions are equal to each other at all pressures.

Material and Impurity	dE/dP (meV/kbar)	Reference
Si:As	– 0.046 ± 0.002	Reference 7
	– 0.1 ± 0.05	Reference 9
Si:In	+ 0.05 ± 0.005	Reference 7
Si:Al	+ 0.01 ± 0.001	Reference 7
Si:B	+ 0.1 ± 0.1	Reference 9
Si:S	– 1.7±0.1 (S^0)	Reference 10
	– 2.05 ± 0.1 (S^+)	
Si:Se	– 1.8 ± 0.1 (Se^0)	Reference 10
	– 2.1 ± 0.1 (Se^+)	
Si:Te	– 0.9 ± 0.05 (Te^0)	Reference 10
	– 1.2 ± 0.05 (Te^+)	
Si:Au	– 1.2 (at low pressure (< 4 kbar)	Reference 8
	– 1.5 (at high pressure (25 kbar))	
	– 2.6 ± 0.5	Reference 9
GaP:S and GaP:Te	+ 0.045 or – 0.023[a]	Reference 11
n-type InP	~ + 0.01 (< 10 kbar)	Reference 17
n-type InAs	– 0.077	Reference 19
n-type GaAs	+ 0.045 (at 1 bar)[b]	Reference 14
GaAs:Si	– 0.05[c] (> 40 kbar)	Reference 23
GaAs:Sn	+ 0.014[c] (> 40 kbar)	Reference 23
AlSb:Te	– 0.13	this work
AlSb:Se	– 1.8 (at 1 bar)	this work
	– 0.2 (at 60 kbar)	

[a]The result depends on the parameters used in obtaining this pressure derivative from the observed 1s(Γ_1) to 1s(Γ_{12}) intergroundstate transition.

[b]Estimated from variation of effective mass and dielectric constant with pressure.

[c]Pressure dependence of a ground to bound-excited state transition.

Table 1

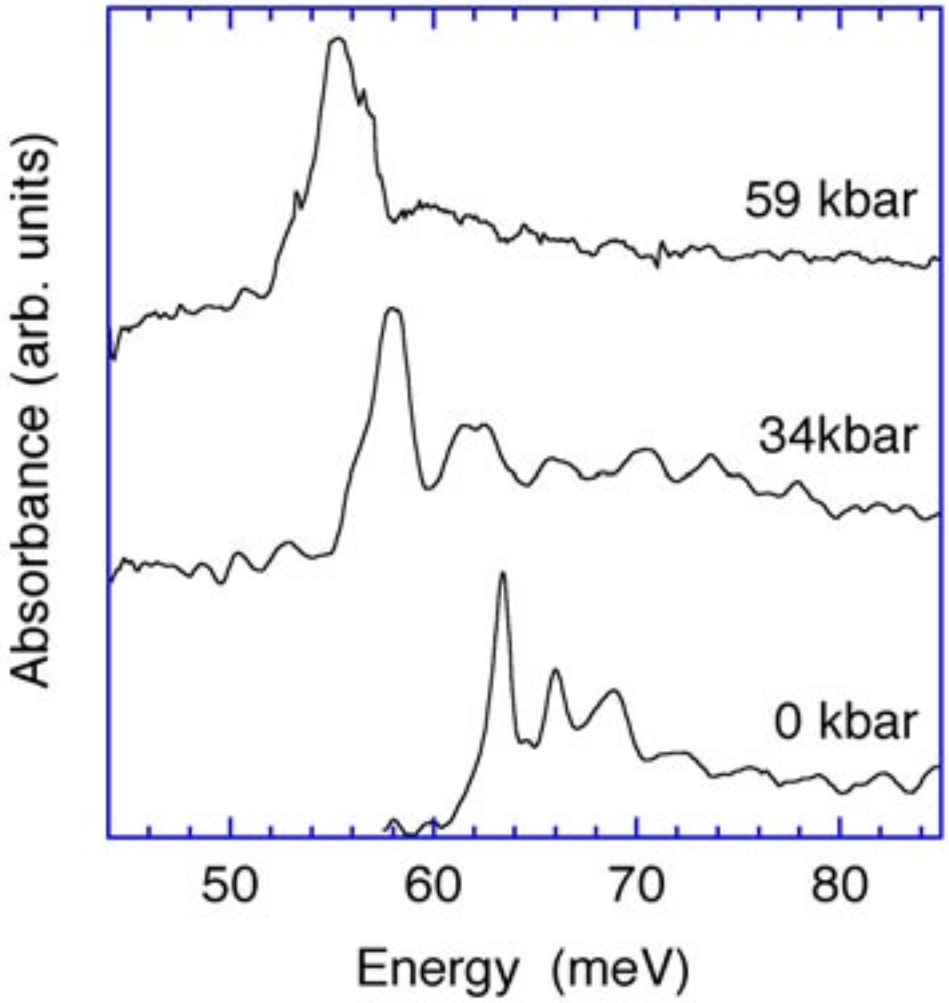
Absorbance (arb. units)
59 kbar
34kbar
0 kbar
50
60
70
80
Energy (meV)

Figure 1

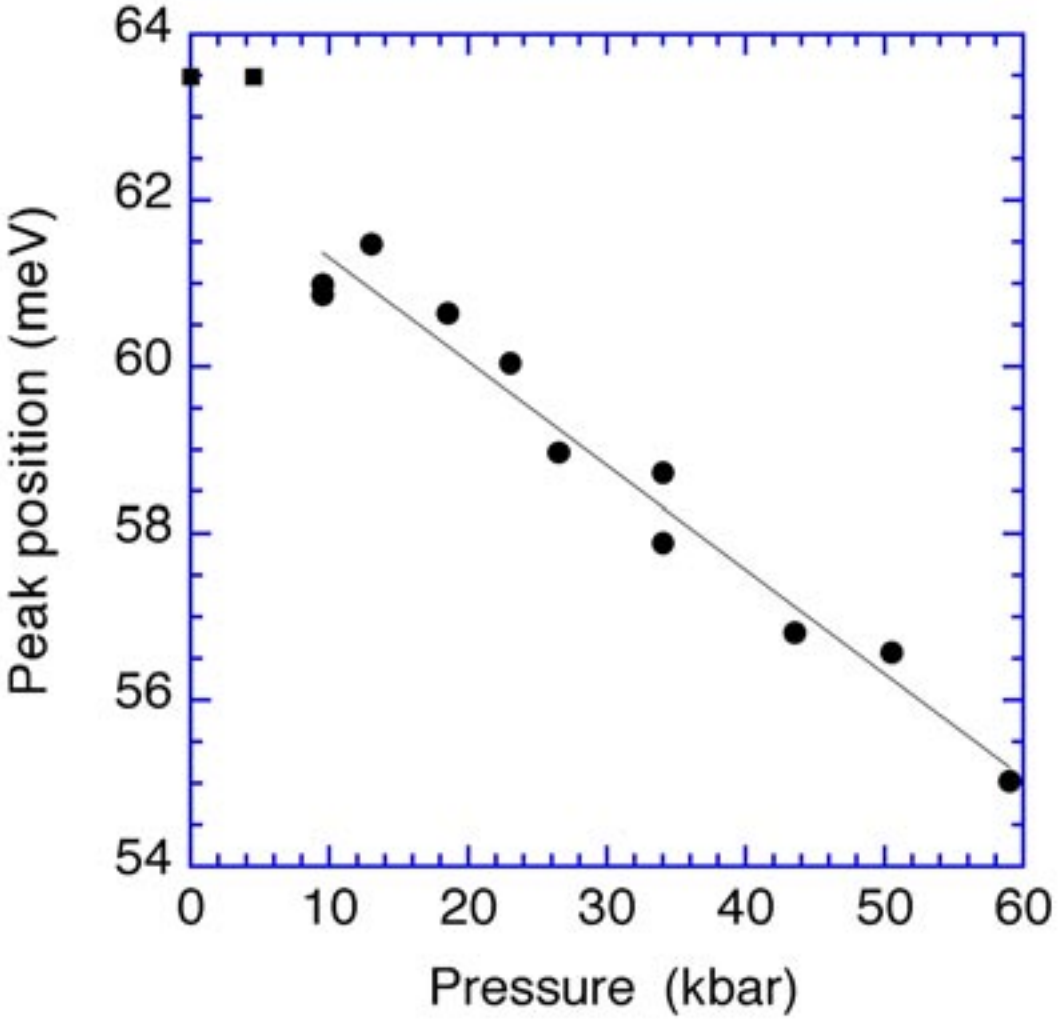
64
62
60
58
56
54
Peak position (meV)
0
10
20
30
40
50
60
Pressure (kbar)

Figure 2

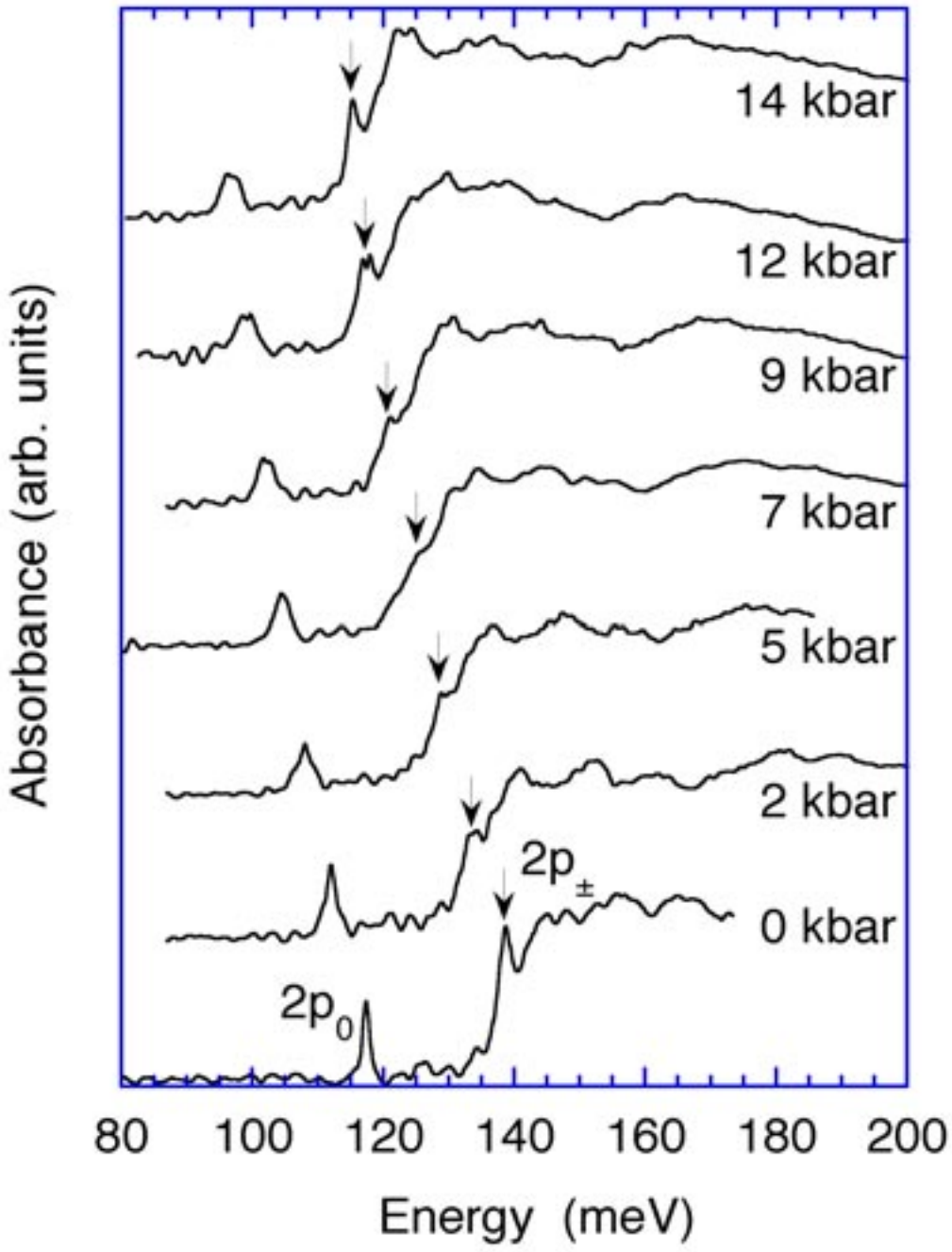
14 kbar
12 kbar
9 kbar
7 kbar
5 kbar
2 kbar
0 kbar
2p±
2p0
Absorbance (arb. units)
80
100
120
140
160
180
200
Energy (meV)

Figure 3

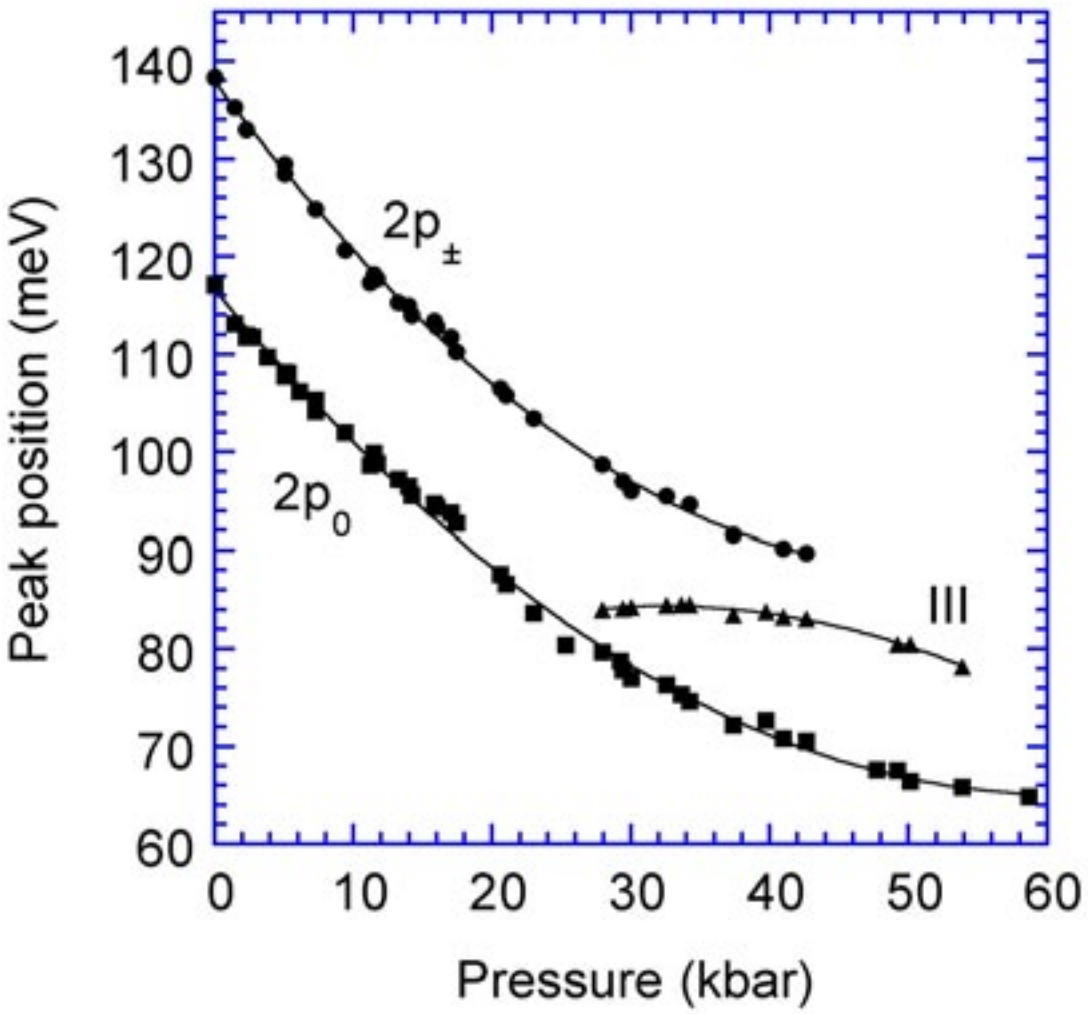
Peak position (meV)
140
130
120
110
100
90
80
70
60
0
10
20
30
40
50
60
Pressure (kbar)
2p±
2p0
III

Figure 4

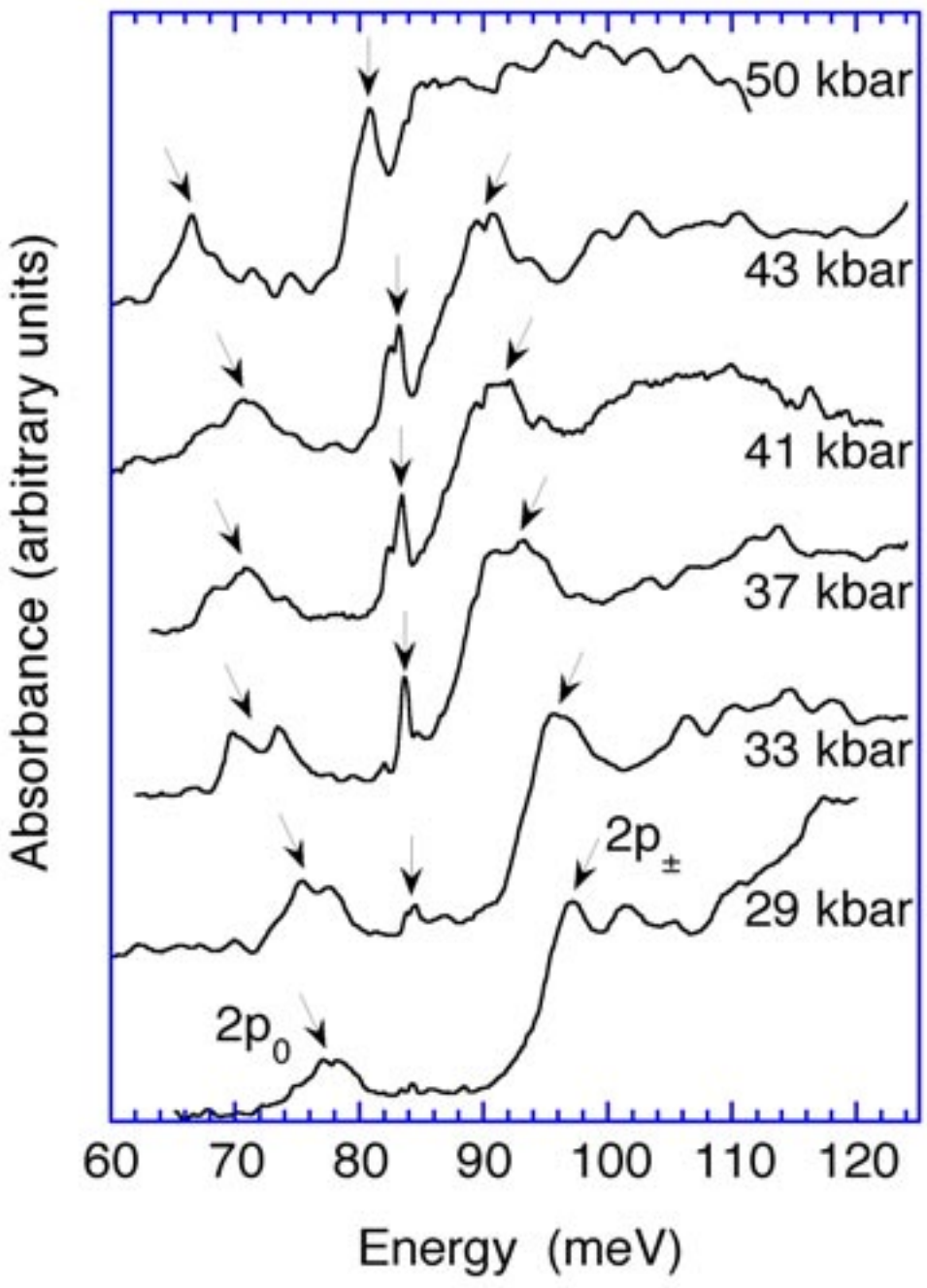
50 kbar
43 kbar
41 kbar
37 kbar
33 kbar
29 kbar
2p±
2p0
Absorbance (arbitrary units)
60
70
80
90
100
110
120
Energy (meV)

Figure 5

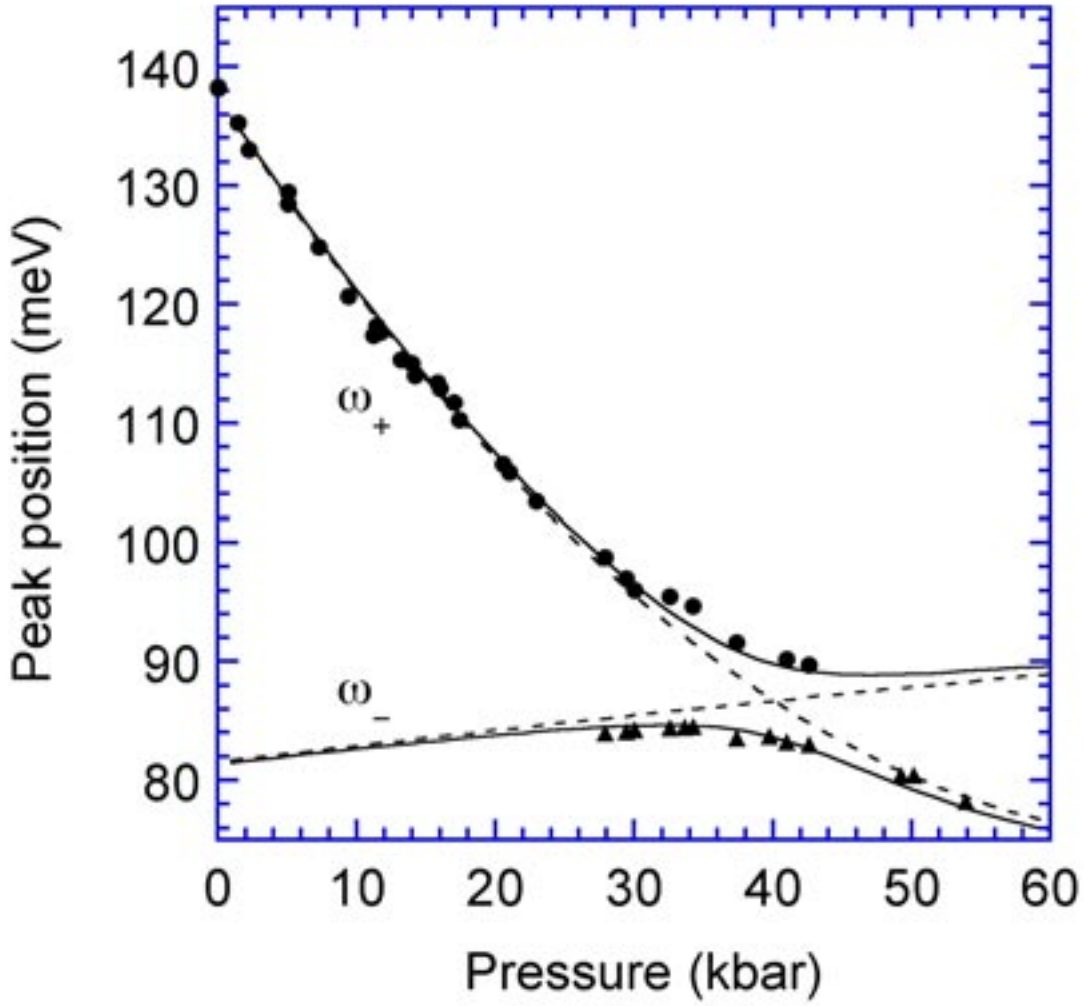
Peak position (meV)
140
130
120
110
100
90
80
ω+
ω−
0
10
20
30
40
50
60
Pressure (kbar)

Figure 6

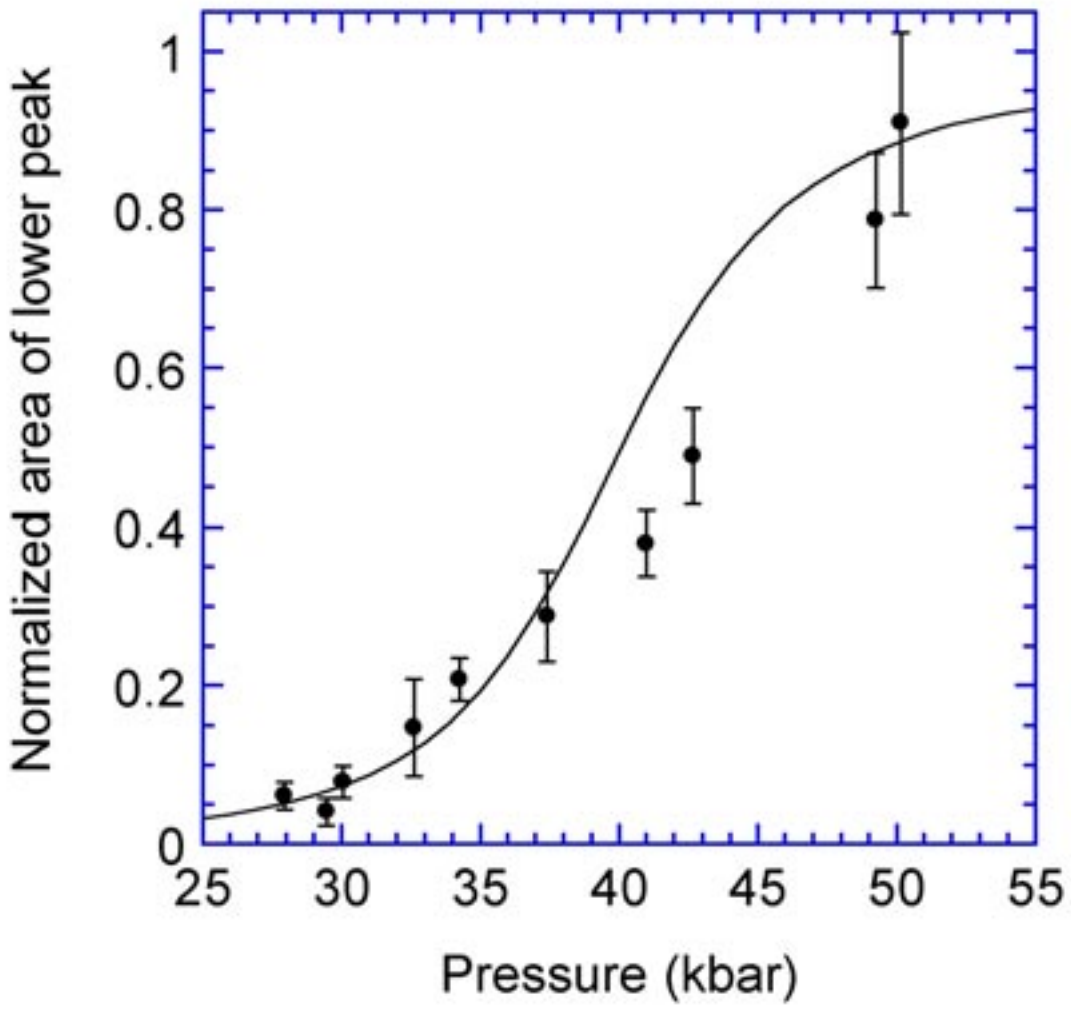
Normalized area of lower peak
0
0.2
0.4
0.6
0.8
1
25
30
35
40
45
50
55
Pressure (kbar)

Figure 7